Ellipsometric study of undersaturated critical adsorption

Jae-Hie J. Cho and Bruce M. Law
Condensed Matter Laboratory, Department of Physics, Kansas State University, Manhattan, Kansas 66506-2601
(Received 23 July 2001; revised manuscript received 20 September 2001; published 17 December 2001)

At the liquid-vapor surface of a critical *AB* binary liquid mixture, if the surface energies $\sigma_A \ll \sigma_B$, then component *A* completely saturates the surface and one is in the regime of strong critical adsorption where the local volume fraction at the surface is solely a function of z/ξ where ξ is the bulk correlation length and z is the depth into the liquid. If, however, $\sigma_A \approx \sigma_B$ then the surface composition is a sensitive function of the surface energy difference $\Delta\sigma = \sigma_A - \sigma_B$ and the surface is ''undersaturated.'' We study this undersaturated critical adsorption regime using a homologous series of critical binary liquid mixtures. Component *B* (methyl formate) is fixed, while component *A* is varied from *n*-undecane to *n*-tetradecane. With increasing carbon chain length $\Delta\sigma$ changes systematically from a negative to a positive value. We find that the experimental results, in both the one- and two-phase regions, are well described by a universal surface scaling function $G(z/\xi, \mathbf{h}_1 t^{-\Delta_1})$, where $\mathbf{h}_1 \sim \Delta\sigma$, $t = |T_c - T|/T_c$ is the reduced temperature relative to the critical temperature (T_c), and Δ_1 is a universal surface critical exponent. These results are in conformity with theoretical predictions.

DOI: 10.1103/PhysRevE.65.011601 PACS number(s): 68.03.Cd, 64.60.Fr

I. INTRODUCTION

The surface critical behavior that occurs at the interface between a noncritical spectator phase and an adjacent critical system is governed by the appearance of universal surface critical exponents and universal surface scaling functions. These universal features are a consequence of the boundary conditions placed upon a semi-infinite three-dimensional system [1,2]. Hence, such features are very common and are found at all noncritical interfaces adjacent to critical systems. For example, boundary conditions determine (i) the variation in the local density at the interface between a container wall and a critical pure fluid, (ii) the preferential adsorption and its variation with depth at the liquid/vapor surface of critical binary liquid mixtures or critical binary alloys, and (iii) the surface orientational order between a uniaxial ferromagnet and a neighboring noncritical phase [3]. Perhaps the most well-studied example for this type of surface critical behavior is critical adsorption, which occurs at the interface between a critical binary liquid mixture and, for example, the (noncritical) vapor phase or a container wall. In critical adsorption the component that possesses the lowest surface energy preferentially adsorbs at the surface. For strong critical adsorption in an *AB* mixture, the surface energies differ greatly, $\sigma_A \ll \sigma_B$, and component *A* almost completely saturates the first few monolayers of the interface (at $z=0$). However, this surface saturated layer must decay with depth z ($\geqslant 0$) to the bulk critical composition over a distance governed by the bulk correlation length $\xi_\pm = \xi_{o\pm} t^{-\nu}$, where the subscript $+$ $(-)$ corresponds to a quantity in the one- (two-) phase region of the liquid mixture, ν (=0.632 [4]) is a universal bulk critical exponent, $t = |T - T_c|/T_c$ is the reduced temperature relative to the critical temperature T_c, and the system dependent amplitude $\xi_{o\pm}$ has a universal amplitude ratio $R_\xi = \xi_{o+}/\xi_{o-}$ ($\simeq 1.96$ [5]). The variation in composition with depth is governed by a universal surface scaling function $P_\pm \equiv P_\pm(z/\xi_\pm)$, which acquires differing forms in the one- and two-phase regimes. More specifically, the local order parameter $m(z)$, which governs the local volume fraction $v(z)$ of the adsorbed component (relative to its critical value v_c) is given by [6,7]

$$m_\pm(z) = v(z) - v_c \tag{1}$$

$$= M_- t^\beta P_\pm(z/\xi_\pm), \tag{2}$$

where $M_- t^\beta$ describes the shape of the coexistence curve, β ($= 0.328$ [4]) is another universal critical exponent, and

$$P_+(\infty) = 0 \quad \text{and} \quad P_-(\infty) = 1 \tag{3}$$

in order to conform with the behavior of the order parameter in the bulk ($z/\xi_\pm \to \infty$). Although the universal surface scaling function $P_\pm$ was predicted to exist more than 20 years ago [6], it has only been in the last few years that theoretical estimates of this function have become available [8–10], which provide reasonable (but not exact) agreement with recent experimental measurements [11,12]. Corrections to scaling [13] may be able to explain this discrepancy between theory and experiment.

A more complicated situation arises if the two components, *A* and *B*, of the liquid mixture possess similar surface energies ($\sigma_A \approx \sigma_B$); now the first few monolayers will no longer be completely saturated with one of the components, and one is in the regime of weak or competitive adsorption. Critical adsorption now depends upon an effective surface field

$$\mathbf{h}_1 \sim \sigma_A - \sigma_B \tag{4}$$

[which will be defined more precisely below, Eq. (21)] and the local order parameter takes the form [6]

$$m_\pm(z) = M_- t^\beta G'_\pm(z/\xi_\pm, \mathbf{h}_1 t^{-\Delta_1}) \tag{5}$$

$$= M_- t^\beta G_\pm(z/\xi_\pm, z/l_{h\pm}), \tag{6}$$

where $G'_\pm = G'_\pm(x,y')$ and $G_\pm = G_\pm(x,y)$ are generalized surface scaling functions. The transformation from Eq. (5) to Eq. (6) involves a simple change of variables where y

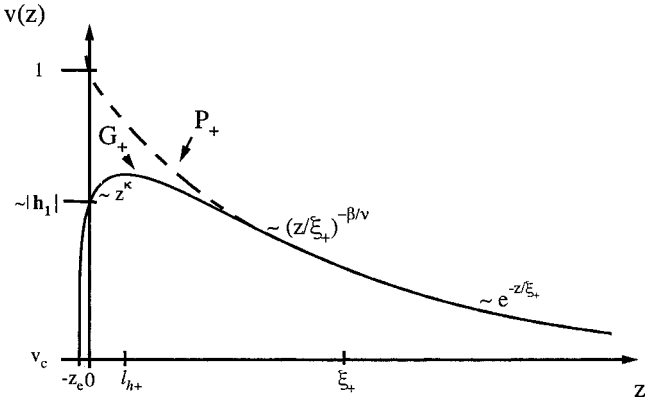

FIG. 1. Schematic plot of the local volume fraction $v(z)$ as a function of depth z into an *AB* critical liquid mixture in the one-phase region. If the surface energy $\sigma_A \ll \sigma_B$ then the surface is completely saturated with component A [$v(0)=1$] and $v(z)$ is described by the surface scaling function P_+ (dashed line), for strong critical adsorption, which varies as $\sim(z/\xi_+)^{-\beta/\nu}$ for $z \lesssim \xi_+$ and $\sim e^{-z/\xi_+}$ for $z \gtrsim \xi_+$. If, however, $\sigma_A \lesssim \sigma_B$ the surface is no longer completely saturated with component A and, in fact, $v(0) \sim |\mathbf{h}_1|$ where the surface field $\mathbf{h}_1 \sim \sigma_A - \sigma_B$ [Eq. (21)]. In this case, $v(z)$ is described by the surface scaling function G_+ (solid line) where $G_+ \sim z^\kappa$ for $z \lesssim l_{h+}$ [$\sim |\mathbf{h}_1|^{-\nu/\Delta_1}$, Eq. (7)], which crosses over to the P_+ function for $z > l_{h+}$. An extrapolation length z_e [see Eq. (31) and Sec. IV for details] ensures that $v(0)=1$ for the P_+ function and $v(0) \sim |\mathbf{h}_1|$ for the G_+ function. In the limit of very large $\mathbf{h}_1$, $l_{h+} \to 0$ and the G_+ function is coincident with the P_+ function.

$= z/l_{h\pm} = xy'^{\nu/\Delta_1}$ and, therefore, the new length scale associated with the $\mathbf{h}_1$ field is given by

$$l_{h\pm} = \xi_{o\pm} |\mathbf{h}_1|^{-\nu/\Delta_1}, \tag{7}$$

which acquires slightly differing values in the one-and two-phase region. The surface critical exponent Δ_1 is discussed in more detail in the following section. In the limit of a strong surface field, which is schematically represented by $\mathbf{h}_1 \to \pm\infty$ [where the $+$ $(-)$ sign corresponds to $B(A)$ adsorption, according to Eq. (4)], the surface scaling functions $G_\pm$ and $G'_\pm$ become insensitive to the specific value of $\mathbf{h}_1$ and these functions crosses over to the strong surface scaling function, namely,

$$G'_\pm(z/\xi_\pm, \pm\infty) = G_\pm(z/\xi_\pm, \pm\infty) = P_\pm(z/\xi_\pm). \tag{8}$$

The variation in the local order parameter $m(z)$, within the one-phase region of a critical mixture, is schematically depicted in Fig. 1 when a weak surface field is present. According to theory (Sec. II, [14]), the surface order parameter at the interface $m_1 = m(z=0) \sim \mathbf{h}_1$ increases with increasing z as $m(z) \sim z^\kappa$, where $\kappa = (\Delta_1 - \beta)/\nu \simeq 0.21$ for $0 < z \lesssim l_{h+}$. At distances greater than l_{h+}, the local order parameter $m(z)$ crosses over to the $P_+(z/\xi_+)$ surface scaling function, where, for $l_{h+} \lesssim z \lesssim \xi_+$ the power law behavior $m(z) \sim z^{-\beta/\nu}$ [6] is found while at larger distances $m(z) \sim e^{-z/\xi_+}$ [7]. The maximum in $m(z)$, which occurs at $z \approx l_{h+}$ (Fig. 1) is an unusual feature that arises naturally from the small $[m(z) \sim z^\kappa]$ and medium $[m(z) \sim z^{-\beta/\nu}]$ z behavior. With increasing $\mathbf{h}_1$, the surface order parameter $m_1(\sim \mathbf{h}_1)$ increases while, at the same time, l_{h+} $[\sim \mathbf{h}_1^{-\nu/\Delta_1}$, Eq. (7)] decreases towards zero and thus, in the limit of an infinitely strong field $(\mathbf{h}_1 \to \infty)$, $m(z)$ is completely described by the strong field surface scaling function $P_+(z/\xi_+)$. One can qualitatively understand therefore, from the representation provided in Fig. 1, that $G_\pm$ differs from $P_\pm$ only very close to the interface at $0 \lesssim z \lesssim l_{h\pm}$. Therefore, weak field effects will be more evident for larger $l_{h\pm}$ [corresponding to smaller $\mathbf{h}_1$, Eq. (7)], namely, for systems with very similar surface energies for the two components *A* and *B* compared with the thermal energy.

Desai, Peach, and Franck [15] conducted the first innovative experimental study into the weak critical adsorption regime. They studied the critical mixture carbon disulfide and nitromethane in contact with a heavily silylated glass surface. The silylated layer, on the glass surface, slowly degraded (or became hydroxylated due to adsorption of water) over a period of 11 days; the adsorption preference consequently changed continuously from strongly carbon disulfide on day 1 to strongly nitromethane by day 11. Around day 5 the surface field was very small and the adsorption of both components was approximately equally probable. The weak field data resulting from this experiment seemed, at first glance, to be at variance with theoretical expectations. This stimulated a flurry of theoretical work [14,16–18], which subsequently provided a qualitative explanation [19] of the weak field experimental results. For this critical mixture solid surface system it was not possible to quantify the magnitude of the surface field $\mathbf{h}_1$ as the adsorption preference changed; this lack of information precluded a quantitative comparison between theory and experiment.

Recently we have approached this interesting weak field regime from a slightly different perspective [20]. We examined the liquid-vapor critical adsorption behavior for a homologous series of critical binary liquid mixtures where one component, *B* (methyl formate), remained fixed while the other component, *A*, was varied from *n*-undecane (denoted C11) to *n*-tetradecane (C14). In this system $\sigma_A \approx \sigma_B$ and the adsorption preference at the liquid-vapor surface changed from *n*-alkane to methyl formate with increasing carbon chain length. Thus, this homologous series of critical mixtures allowed us to tune the $\mathbf{h}_1$ field from negative to positive values with increasing chain length while, at the same time, providing a quantitative measure of the magnitude of $\mathbf{h}_1$ through the difference in surface tensions between the two components. Thus, in this case, it was possible to quantitatively compare theoretical predictions for the surface scaling function G_+ with experiment, at least, in the one-phase region. The purpose of this paper is to expand upon our earlier work within the one-phase region and also to analyze the more complicated two-phase critical adsorption behavior in these weak field systems. This paper is set out as follows. In Sec. II we outline the theoretical predictions and provide an *Ansatz* that conforms with these predictions. The experimental methods and results are given in Sec. III while the ellipsometric data is analyzed in Sec. IV. Finally, the surface field $\mathbf{h}_1$ and its connection with the surface energy difference σ_A

$-\sigma_B$ is placed on a quantitative basis in Sec. V and the findings from this research are summarized in Sec. VI.

II. THEORETICAL CONCEPTS

The theoretical work surrounding critical adsorption is very extensive and covers many different topics, where a number of these topics are *not* directly relevant to experimental systems. There are a number of excellent, but somewhat older, reviews of critical adsorption and its relationship to wetting and other related surface critical phenomena [1–3]. More recent theoretical advances are reviewed in [21] while [22] provides an overview of recent experimental developments. For the first time reader or experimentalist, who is entering this field, the theoretical literature can be somewhat forbidding. Hence, in this section, we provide a brief guide to the nomenclature and concepts relevant for both strong and weak critical adsorption.

Critical phenomena is frequently modeled using lattice models where the dimensionless neighbor-neighbor bond strength (normalized by the thermal energy k_BT) is $K=J/k_BT$, where, within the first surface layer at $z=0$ the bond strength may differ from its bulk value and is therefore represented by $K_1=J_1/k_BT$. In the absence of any bulk field ($h=0$) and for zero surface field ($h_1=0$), surface ordering can only be generated by the strength of K_1 relative to K; hence the surface enhancement parameter [1]

$$c\sim(K-K_1) \tag{9}$$

is a relevant variable to consider. For $K_1\gg K$ the surface is strongly ordered, relative to the bulk, and the bulk undergoes a disorder-order transition in the presence of an *ordered* surface at the bulk critical temperature T_c. This transition is called the *extraordinary transition* at the renormalization group (RG) fixed point $c\rightarrow-\infty$. Conversely, in the other extreme, for $K_1\ll K$ the surface is *less ordered* relative to the bulk; at the RG fixed point $c\rightarrow+\infty$, the surface transition at T_c is called the *ordinary transition*. Alternatively, at a specific value of c designated by $c_{\rm sp}$ (with $K_1\simeq 1.5$ K [23]), the surface *attains criticality* at the bulk critical temperature T_c; this surface transition is called the *special transition*. The extraordinary, ordinary, and special transitions each acquire differing surface critical exponents. For the extraordinary transition, values for these surface critical exponents can be deduced from Refs. [24,25], while for the ordinary and special transitions they have been recently summarized in [26].

The surface can also become ordered via another mechanism, which differs from that which occurs at the extraordinary transition ($c\rightarrow-\infty, h_1=0$). For $c\rightarrow+\infty$, where in the absence of a surface field ($h_1=0$) the surface is less ordered than the bulk (ordinary transition), *enhanced surface order* can be induced by the presence of a strong surface field h_1, which acts solely upon the surface atoms at $z=0$. In the limit of $|h_1|\rightarrow\infty$ (and $c\rightarrow+\infty$) the surface transition that occurs at T_c is called the *normal transition* [27]. For critical binary liquid mixtures, surface ordering corresponding to critical adsorption is thought to be induced by the presence of a surface field and, therefore, *strong critical adsorption should be described by the normal transition*. More specifically, atoms in the surface possess a lower coordination number (compared with the bulk), which is expected to lead to decreased order on approaching the surface ($c\gg 0$), however, the presence of a surface field ($|h_1|>0$) may compensate for this lower coordination and give rise to an enhanced surface ordering. Many years ago Bray and Moore [28] suggested that the surface ordering induced at the extraordinary transition ($c\rightarrow-\infty, h_1=0$) should be equivalent to the surface ordering induced at the normal transition ($c\rightarrow\infty, |h_1|\rightarrow\infty$). This equivalence between the extraordinary and normal transitions has recently been demonstrated to be rigorously true [24,25]. This one-to-one correspondence therefore allows theoretical results, derived for the extraordinary transition, to be applied to the normal transition. Indeed, the experimental surface scaling function $P_{\pm}$, which describes strong critical adsorption [11,12], was found to exhibit the expected power law behavior

$$P_{\pm}(x)\sim c_{\pm}x^{-\beta/\nu}, \quad 0<x\lesssim 1 \tag{10}$$

at mesoscopic distances from the interface, which at large distances, crossed over to exponential decay

$$P_{\pm}(x)\sim P_{\infty\pm}e^{-x}, \quad x\gtrsim 1, \tag{11}$$

in agreement with the expectations of the extraordinary transition [8]. In Eqs. (10) and (11) $c_{\pm}$ and $P_{\infty\pm}$ are universal numbers because $P_{\pm}(x)$ is a universal function.

In reality, a value of $|h_1|\rightarrow\infty$ (present at the normal transition) is unrealistic; all real systems will possess a finite (but perhaps large) surface field h_1. Therefore new surface phenomena, characterized by ordinary surface critical exponents (because $c\gg 0$), are expected to become apparent at distances $0\lesssim z\lesssim l_h$ [$\sim h_1^{-\nu/\Delta_1}$, Eq. (7) and Fig. 1]. Optical reflectometry [29], ellipsometry ([30,11,12] and references therein), neutron reflectometry [31], and evanescent-wave light scattering [32] have been used to study strong critical adsorption ($\sigma_A\ll\sigma_B$). In all of these experiments there has been no conclusive evidence for the presence of this new surface regime characterized by ordinary surface critical exponents. This is perhaps not surprising because these techniques typically measure an integral over the surface structure; for example, sufficiently far from T_c, ellipsometry measures the relative adsorption $\Gamma\sim\int_0^{\infty}[v(x)-v_c]dx\sim\int_0^{\infty}[P_{\pm}(x)-P_{\pm}(\infty)]dx$ [33,34]. Therefore, these techniques are sensitive to surface structure on all length scales, and, especially on large length scales ($z\sim\xi$) away from the regime where ordinary surface critical exponents occur. By contrast, evidence for the presence of ''ordinary'' surface critical exponents were evident in surface tension measurements [35,36] conducted within the two-phase region of critical binary liquid mixtures [37]. These measurements provided a measure of the surface critical exponent Δ_1 whose experimental value (0.43 ± 0.05 [35], 0.44 ± 0.06 [36]) is in good agreement with the ordinary value $\Delta_1^{\rm ord}=0.464$ [26], which differs significantly from either the extraordinary ($\Delta_1^{ex}=-\nu=-0.632$ [38]) or special ($\Delta_1^{\rm sp}=0.997$ [26]) surface critical exponents. A discussion of the interrelationship between critical adsorp-

tion and surface tension measurements, within critical binary liquid mixtures, can be found in [22]. Henceforth, throughout the remainder of this paper surface critical exponents, such as Δ_1 and β_1 will always refer to ordinary surface critical exponents.

As argued in the Introduction, this surface regime, in which ordinary surface critical exponents play an important role, will become more prominent for larger l_h ($\sim h_1^{-\nu/\Delta_1}$) and hence for smaller h_1. Ritschel and co-workers [14,16,17] considered this small surface field regime in detail. Essentially they found the following.

(i) For small h_1 and large c (i.e., close to the fixed point of the ordinary transition), the parameter c is a ''dangerous irrelevant variable,'' which cannot be naively set to its fixed point value of $c=\infty$; instead, the effective surface field that acts on the system is $\mathbf{h}_1=h_1/c^y$, where y is a critical exponent. The effective surface field $\mathbf{h}_1$ is the parameter that appears in the surface scaling functions $G'_{\pm}$ [Eq. (5)] and $G_{\pm}$ [Eqs. (6) and (7)].

(ii) As $\mathbf{h}_1\to\infty$, the local order parameter $m(z)$ must be described by the strong field surface scaling function, namely, $P_{\pm}$ [Eq. (2)], in both the one- and two-phase regions.

(iii) In the one-phase region, for $\mathbf{h}_1$ finite, the following holds.

(a) For $z\gg l_{h+}$ the local order parameter $m(z)$ must be described by the P_+ function.

(b) For $0<z\ll l_{h+},\xi_+$, then,

$$m(z)\sim\mathbf{h}_1 z^{\kappa},\quad \kappa=(\Delta_1-\beta)/\nu\simeq 0.21. \tag{12}$$

(c) At $\mathbf{h}_1=0$ the local order parameter $m(z)=0$ for all z, while at small $\mathbf{h}_1$, then, $G_+\sim\mathbf{h}_1$.

(iv) At T_c, the local order parameter is continuous, namely,

$$m_+(z)=m_-(z). \tag{13}$$

This equality imposes a constraint on the relationship between G_+ and G_- as described below.

(v) In the two-phase regime for $\mathbf{h}_1=0$ and $0<z\ll l_{h-},\xi_-$,

$$m(z)\sim z^{(\beta_1-\beta)/\nu}t^{\beta_1}, \tag{14}$$

where $\beta_1=0.803$ [26] for the ordinary transition.

Conditions (i)–(v) are a consequence of simple scaling considerations near a continuous bulk phase transition [14]. These results have been checked against surface RG calculations to order ϵ [14,16] and Monte Carlo simulations in three dimensions [17], as well as, exact results and Monte Carlo simulations in two dimensions [18,19,39]. Additionally, various generalizations of this weak field case to the situation where *both* h_1 and c are small, in the vicinity of the special transition, have been considered [16].

It is possible to construct a number of different *Ansätze* that conform with conditions (i)–(v) above. In the spirit of Liu and Fisher [7], we expect that a simple crossover function between the various asymptotic regions will provide a good theoretical description with which to compare experimental data. In [20], a simple ''algebraic'' crossover between the asymptotic regimes described the one-phase weak critical adsorption data well. However, in subsequent unpublished work this algebraic crossover function had difficulties describing the two-phase experimental data. In this paper we consider an ''exponential'' crossover model, which describes both the one-and two-phase regions well. In this model

$$G_{\pm}(x,y)=[1-(1-X_{\pm})(1-Y)]P_{\pm}(x), \tag{15}$$

$$X_+=0,\quad X_-=(1-e^{-x})^{x_1}, \tag{16}$$

$$Y=(1-e^{-y})^{y_1}, \tag{17}$$

$$x_1=\beta_1/\nu,\quad y_1=\Delta_1/\nu, \tag{18}$$

$$x=\frac{z+z_e}{\xi_{\pm}},\quad y=\frac{z+z_e}{C_{\pm}l_{h\pm}}, \tag{19}$$

$$C_+=1,\quad C_-=\xi_{o+}/\xi_{o-}\equiv R_{\xi}, \tag{20}$$

$l_{h\pm}$ is described by Eq. (7), and

$$\mathbf{h}_1=\frac{(\sigma_A-\sigma_B)l_{\sigma}^2}{k_BT_c}. \tag{21}$$

Equations (15)–(21) conform with conditions (i)–(v). An extrapolation length z_e has been introduced into Eq. (19). It services two purposes, as discussed in Sec. IV [Eq. (31)]: it ensures that $P_{\pm}$ remains finite at $z=0$ and it guarantees that $m_{\pm}(z=0)\sim\mathbf{h}_1$ for small $\mathbf{h}_1$, in conformity with condition (iii c). A constant C_- appears in Eq. (19); it arises from the continuity condition at T_c [condition (iv)], where the continuity of $P_{\pm}$ must also be taken into consideration [40]. As discussed in the Introduction, the surface field $\mathbf{h}_1$ should be proportional to $\sigma_A-\sigma_B$ where σ_A (σ_B) corresponds to the liquid-vapor surface energy of the *n*-alkane (methyl formate) component *within* the liquid mixture; hence, if $\mathbf{h}_1<0$ (>0) the *n*-alkane (methyl formate) preferentially adsorbs at the liquid/vapor surface and $v(z)$ represents the local volume fraction of *n*-alkane (methyl formate). The surface field $\mathbf{h}_1$ [Eq. (21)], which is normalized by the thermal energy at T_c, has been made dimensionless by introducing a new noncritical length scale l_{σ}. This length scale is expected to be system dependent and of the order of a molecular length. In using this model for $G_{\pm}$, a reasonable form must be selected for $P_{\pm}$. Throughout this paper we have chosen to use the P3a model from [12] for the $P_{\pm}$ function, however, any of the $P_{\pm}$ models contained within [11,12] could have been used with essentially identical results for $G_{\pm}$ as obtained here.

III. EXPERIMENTAL METHODS

Complete adsorption occurs at the liquid-vapor surface of a critical binary liquid mixture if a sufficiently strong surface field, $\mathbf{h}_1$, is present; under such conditions the first few layers are saturated with the component possessing the lowest surface energy. A strong surface field is relatively easy to obtain—the components merely have to possess a suffi-

TABLE I. Liquid mixture material parameters.

Mixture	ε_A[a]	ε_B[a]	M_-	ξ_{0+}[b] (Å)	$\Delta\sigma$ (erg/cm^2)	v_{cA}	T_c (°C)
C11	1.994	1.793	0.95 ± 0.10	2.2 ± 0.2	-1.657	0.478	26.975
C12	2.000	1.786	0.93 ± 0.02	2.0 ± 0.2	-0.559	0.465	32.713
C13	2.006	1.781	0.98 ± 0.07	2.1 ± 0.3	0.424	0.460	37.473
C14	2.009	1.775	0.98 ± 0.04	2.3 ± 0.4	1.371	0.451	42.662

[a]Optical dielectric constant from Ref. [61] recalculated at T_c, where subscript A denotes *n*-alkane and B is methyl formate. Note that the *n*-alkane is the lighter component for all of the liquid mixtures.
[b]Measured via turbidity.

ciently large surface tension difference (e.g., $|\Delta\sigma|=|\sigma_A-\sigma_B|\gtrsim 10$ erg/cm^2) and, in fact, this was one of the primary considerations that we used in selecting appropriate critical liquid mixtures in our prior studies of strong critical adsorption [30,11]. A second important consideration, which influenced our previous choice of critical binary liquid mixtures, was to select mixtures where the *lighter* component possessed the lowest surface tension—such a condition guarantees that we can study strong critical adsorption, not only in the one-phase region, but also in the two-phase region [41].

Obviously, from the form of $G_\pm(x,y)$ [Eq. (15)] given in the preceding section, it is imperative that the strong critical adsorption surface scaling function $P_\pm$ should be known *very accurately* before the weak critical adsorption surface scaling function $G_\pm$ can be studied. Thus, the current experiments could not have been accurately analyzed and interpreted prior to the work of Carpenter and co-workers [11,12]. For a quantitative study of weak critical adsorption the two components need to possess rather similar surface energies ($\sigma_A\approx\sigma_B$) where preferrably one component is, for example, an *n*-alkane so that a homologous sequence of critical binary liquid mixtures possessing slightly differing surface fields can be studied. Additionally, the critical temperatures of these mixtures should be in a convenient temperature range near room temperature. Critical binary liquid mixtures of an *n*-alkane (*n*-undecane to *n*-tetradecane) and methyl formate fulfill these requirements and thus were selected for this study. With each additional carbon atom, the surface tension of the pure *n*-alkane increases by $\sim$0.5 erg/cm^2; hence, the surface field is expected to increase in small steps with increasing chain length provided that the critical temperature is similar for each of the critical mixtures.

The *n*-alkanes (undecane, dodecane, tridecane, and tetradecane) together with methyl formate (MF) were purchased from Aldrich and used without any further purification. They had a stated purity of more than 99%. Teflon 0.5 μm Millipore filters were used in the preparation of all samples to remove particulates. For each of the critical binary liquid mixtures, many different system dependent parameters must be independently measured in order to reduce the number of unknown parameters in this study of weak critical adsorption. Specifically, M_-, v_c, ξ_{o+}, T_c, and $\Delta\sigma=\sigma_A-\sigma_B$ should be accurately determined for each liquid mixture. In Table I we list these parameters together with the optical dielectric constants ε at a wavelength of $\lambda=632.8$ nm and temperature T_c. In this table the subscript A (B) refers to *n*-alkane (methyl formate) where it is important to note that the density $\rho_A<\rho_B$ for all liquid mixtures—this will be an important issue in the two-phase region where, in fact, wetting occurs for $\Delta\sigma>0$ (i.e., for C13 and C14) [41]. The parameter M_- was extracted from the coexistence curve for each of the liquid mixtures, while the critical volume fraction v_c was determined using the standard technique of finding that volume fraction where the upper and lower phases possessed equal volumes a few millikelvin into the two-phase region. The determination of the effective surface energy difference $\Delta\sigma$ is discussed in Sec. V.

There are many different experimental techniques for determining ξ_{o+}, including static light scattering, dynamic light scattering, and turbidity measurements [42]. Frequently one finds that ξ_{o+} differs by upwards of 30% for the *same* critical liquid mixture when studied by different groups, or, when studied using different techniques. We have found that one of the more accurate methods for determining ξ_{o+} is via an ellipsometric study of strong critical adsorption in the one-phase regime [30,11]. Ellipsometry measures the ellipticity $\overline{\rho}$ at various reduced temperatures t (see below). In the one-phase region, $\overline{\rho}$ exhibits a peak ($\overline{\rho}_{\rm peak}$) whose position is determined by the correlation length ξ_+. On a $\overline{\rho}$ versus ξ_+/λ plot, $\overline{\rho}_{\rm peak}$ occurs at a universal value given by [11]

$$(\xi_+/\lambda)_{\rm peak}=(\xi_{o+}t^{-\nu}/\lambda)_{\rm peak}=0.064\pm0.006. \qquad (22)$$

Hence, for a critical liquid mixture of unknown ξ_{o+}, by determining the value of t where $\overline{\rho}$ exhibits a peak, an accurate value for ξ_{o+} can be determined from Eq. (22).

It is not obvious *a priori* whether or not Eq. (22) continues to hold for weak surface fields. Therefore, ξ_{o+} was determined independently using the technique of turbidity [43] (see Table I). In retrospect, the value of ξ_{o+} calculated from Eq. (22) is in good agreement with both the turbidity results (Table I) and with the results from the G_+ model (Sec. 4 and Table II). Hence, even for weak critical adsorption, Eq. (22) provides a reasonable estimate of ξ_{o+}, provided the surface energy difference $|\Delta\sigma|\gtrsim 0.4$ erg/cm^2—corresponding to the lowest value of $\Delta\sigma$ exhibited in Table I. In hindsight, this can be understood as follows: for the critical liquid mixtures studied in this paper, although $\mathbf{h}_1$ is small, at sufficiently small t (in the vicinity of the $\overline{\rho}$ peak) the scaling variable $\mathbf{h}_1 t^{-\Delta_1}$, which appears in Eq. (5), is rather large; hence, $G'_+(z/\xi_+,\mathbf{h}_1 t^{-\Delta_1})\simeq P_+(z/\xi_+)$ and the ellipticity $\overline{\rho}$ in the vicinity of the peak is well described by the strong surface scaling function P_+ [which was originally used to deduce Eq. (22)].

TABLE II. Weak critical adsorption parameters. $s = \sqrt{\sum_{i=1}^{N}(\overline{\rho_i}-\overline{\rho}_{Gi})^2/(N-3)}$. The following critical exponents/amplitude ratios were used in the fitting procedure: $\beta=0.328$ [4], $\nu=0.632$ [4], $\Delta_1=0.461$ ([26] lists 0.464 as the best value), $\beta_1=0.803$ [26], and $R_\xi \simeq 1.96$ [5].

	$G_\pm$ model ($l_\sigma = 4.6 \pm 0.4$ Å)			
Mixtures	ξ_{BG} (Å)	ξ_{0+} (Å)	l_{h+} (Å)	$10^3 s_{min}$
C11	3.2	2.0	46 ± 1	0.041 225
C12	2.9	1.9	195 ± 47	0.092 137
C13	2.3	1.8	250 ± 83	0.101 856
C14	2.4	1.9	135 ± 6	0.112 136

Ellipsometry and, in particular, phase modulated ellipsometry has proven to be extremely useful in the study of surface phenomena [44,22]. The construction and operation of our phase modulated ellipsometer, used in this study of weak critical adsorption, is similar to the description and operation in [45]. A HeNe laser with wavelength $\lambda = 632.8$ nm is used as the light source where, after appropriate polarization and phase modulation, the reflected beam from the liquid-vapor surface provides a measurement of the ellipticity,

$$\tilde{\rho} \equiv \mathrm{Im}(r_p/r_s)|_{\theta_B}, \tag{23}$$

at the Brewster angle (θ_B). Here r_p and r_s are the reflection amplitudes for polarizations parallel (p) and perpendicular (s) to the plane of incidence and the Brewster angle is operationally defined by that angle of incidence where

$$\mathrm{Re}(r_p/r_s)|_{\theta_B} = 0. \tag{24}$$

Our sample cell is of simple construction. It is composed of a chemically resistant pyrex cylinder of diameter ~2.3 cm and length ~7 cm. The cell is first etched clean using a glass etch (35% HNO_3, 5% HF, and 60% distilled water by volume), rinsed well with double distilled deionized water, dried overnight, and then half filled with the critical mixture before flame sealing. This sample cell is placed inside a two-stage oven composed of a resistively heated inner stage and a water-cooled outer stage. Thermal gradients along the length of the sample cell are less than ~1 mK/cm, while short and long term thermal stabilities are, respectively, ~0.1 mK over 4 h and ~1 mK per day. The critical temperatures for the mixtures were monitored *in situ* by measuring the temperature at which spinodal decomposition occurs (as indicated by the spinodal ring); this allowed T_c to be measured to within ~1 mK (Table I). In a typical ellipsometric measurement, at each temperature, 6 h elapsed to ensure thermal and diffusive equilibrium (the thermal time constant of the oven is actually only ~10 min) and then ten $\overline{\rho}$ and T measurements were collected over the succeeding hour. The results presented in this paper are the average of these ten measurements. The temperature was always decreased in successive measurements, so that gravity assisted the phase separation process. This protocol was followed in the one-phase region for all four liquid mixtures and in the two-phase region for C11 and C12. A different procedure must be followed for C13 and C14, in the two-phase region, where a critical wetting layer, similar to [46], is found [47]. For these two mixtures, the critical adsorption state is a metastable surface state sufficiently close to T_c. Information about this metastable surface state is obtained following a procedure similar to [48]. The system was first heated well above T_c and mixed well to ensure homogeneity—after 2 h in this high temperature state, the temperature was lowered to ~100 mK above T_c where the system was equilibrated for a further hour. Finally, the system was quenched rapidly into the two-phase region to the selected temperature T, while $\overline{\rho}$ was monitored continuously as a function of time. The metastable critical adsorption data was extracted from this quench data, at early times, before droplets had nucleated on the surface [48].

IV. ANALYSIS OF THE ELLIPSOMETRIC DATA

In order to compare a critical adsorption model with the experimentally measured ellipticity $\overline{\rho}$ the local order parameter $m(z) = v(z) - v_c$ must be related to the complex reflection amplitudes r_p and r_s [see Eq. (23)]. This is accomplished as follows. The local volume fraction $v(z)$ of the adsorbed component (here assumed to be component A) is related to the local optical dielectric constant $\varepsilon(z)$ at depth z via the two-component Clausius-Mossotti equation [49]

$$f(\varepsilon(z)) = v(z) f(\varepsilon_A) + [1 - v(z)] f(\varepsilon_B), \tag{25}$$

where the function

$$f(\epsilon) = \frac{\epsilon - 1}{\epsilon + 2}, \tag{26}$$

ε_A and ε_B are the optical dielectric constants of the pure components (Table I), and we have neglected any volume changes due to mixing of the two components (which normally only amount to corrections of the order of 1–2 %). The surface dielectric function $\varepsilon(z)$ is then used to determine r_p and r_s by numerically solving Maxwell's equations [50,51], from which $\overline{\rho} \equiv \mathrm{Im}(r_p/r_s)|_{\theta_B}$ can be obtained. This procedure is repeated for each reduced temperature t and the resulting ellipticity $\overline{\rho}(t)$, from these model calculations, can then be compared with experimental data.

If the surface layer is sufficiently thin compared with the wavelength of light, namely, $\xi/\lambda \ll 1$ (which occurs sufficiently far from T_c, say, $t \gtrsim 5 \times 10^{-3}$ [33,34]) then the Drude equation [52] provides an accurate description of the ellipticity, at least to first order in ξ/λ [53], where

$$\overline{\rho}(t) \simeq \frac{\pi}{\lambda} \frac{\sqrt{\varepsilon_1 + \varepsilon_2}}{\varepsilon_1 - \varepsilon_2} \int_{-\infty}^{\infty} \frac{[\varepsilon(z,t) - \varepsilon_1][\varepsilon(z,t) - \varepsilon_2]}{\varepsilon(z,t)} dz \tag{27}$$

$$\simeq \overline{\rho}_c(\xi(t)) + \overline{\rho}_{BG}(\xi_{BG}), \tag{28}$$

which has been subdivided into a critical contribution $\overline{\rho}_c$ with

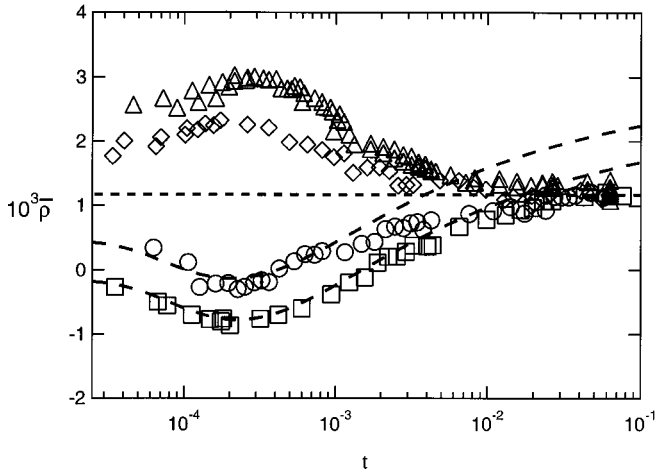

FIG. 2. Ellipticity $\bar{\rho}$ data in the one-phase region for C11 (squares), C12 (circles), C13 (diamonds), and C14 (triangles). The four critical liquid mixtures possess a similar background ellipticity $\bar{\rho}_{\mathrm{BG}}$ at large reduced temperatures t ($\sim 10^{-1}$) due to their similar optical properties. However, at smaller t, the behavior of the four liquid mixtures is distinctly different due to the differing critical adsorption behaviors caused by differing surface fields $\mathbf{h}_1 \sim \sigma_A - \sigma_B$. For C11 and C12, $\bar{\rho}$ deviates below $\bar{\rho}_{\mathrm{BG}}$, which indicates that the *n*-alkane (component *A*) adsorbs at the liquid-vapor surface and $\mathbf{h}_1 < 0$. By contrast, for C13 and C14, $\bar{\rho}$ deviates above $\bar{\rho}_{\mathrm{BG}}$ and it is the methyl formate component (*B*) that preferentially adsorbs at the liquid-vapor surface ($\mathbf{h}_1 > 0$). A liquid mixture where $\mathbf{h}_1 = 0$ would have $\bar{\rho} = \bar{\rho}_{\mathrm{BG}}$ (horizontal dashed line) for all t. The long dashed lines that represent $\bar{\rho}_{P+}$, calculated using the P_+ surface scaling function, demonstrate that this function describes the experimental data well at sufficiently small t where the scaling variable $\mathbf{h}_1 t^{-\Delta_1}$ is large. At large t (corresponding to small $\mathbf{h}_1 t^{-\Delta_1}$) significant deviations from $\bar{\rho}_{P+}$ are observed; the behavior in this regime is accounted for by the G_+ surface scaling function (see text for details).

$$\bar{\rho}_c(\xi(t)) = -\frac{\pi}{\lambda}\frac{\sqrt{\varepsilon_1+\varepsilon_2}}{\varepsilon_2}\int_0^{+\infty}[\varepsilon(z,t)-\varepsilon_2]dz \qquad (29)$$

and a noncritical background contribution $\bar{\rho}_{\mathrm{BG}}$. The liquid-vapor interface is situated at $z=0$ where $\varepsilon(z,t)$ describes the variation in the local optical dielectric constant between the incident medium ($\varepsilon_1 = 1$ for vapor) at $z = -\infty$ and the bulk liquid (ε_2) at $z = +\infty$. On the liquid side of this interface ($z>0$), where critical adsorption occurs, the approximation $|\varepsilon(z,t)-\varepsilon_2| \ll (\varepsilon_2-\varepsilon_1)$ leads to Eq. (29). On the vapor side of this interface ($z<0$), the variation in the local number density of molecules, characterized by a noncritical correlation length ξ_{BG}, gives rise to the background term $\bar{\rho}_{\mathrm{BG}}(\xi_{\mathrm{BG}})$.

Equation (27)–(29) are particularly useful in providing a qualitative understanding of the experimental $\bar{\rho}$ data in the one-phase region (Fig. 2), at least far from T_c; and in estimating the composition of the liquid mixture where the surface field $\mathbf{h}_1 = 0$ (Fig. 3). At sufficiently high temperatures, far from T_c, the correlation length $\xi_+ \to 0$ and $\bar{\rho} \simeq \bar{\rho}_{\mathrm{BG}}$. All four critical liquid mixtures possess similar optical properties (Table I), therefore $\bar{\rho}_{\mathrm{BG}}$ should be similar for all mixtures. This is indeed the case (Fig. 2). The background term is

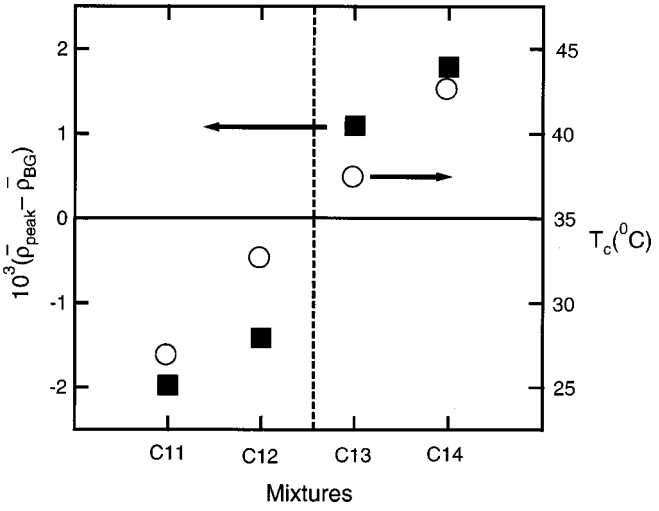

FIG. 3. Graph of $\bar{\rho}_{\mathrm{peak}} - \bar{\rho}_{\mathrm{BG}}$ (solid squares) and critical temperature T_c (open circles) for the various critical mixtures. For zero surface field ($\mathbf{h}_1 = 0$), we expect that $\bar{\rho}_{\mathrm{peak}} = \bar{\rho}_{\mathrm{BG}}$; this occurs at an "effective mixture" of C12.6 with a critical temperature T_c (C12.6) = 35.4 °C.

positive, $\bar{\rho}_{\mathrm{BG}} \simeq 1.17 \times 10^{-3}$ (estimated by averaging the data at $t \gtrsim 5 \times 10^{-2}$ for the four liquid mixtures), because $\varepsilon_1 < \varepsilon(z) < \varepsilon_2$ far from T_c; thus, the integral in Eq. (27) is negative and hence $\bar{\rho} \simeq \bar{\rho}_{\mathrm{BG}}$ is positive. For smaller t, the experimental data indicates that the critical contribution ρ_c is negative (positive) for C11 and C12 (C13 and C14) corresponding to *n*-alkane (MF) adsorption at the liquid-vapor surface [as $\varepsilon_A > \varepsilon_B$ (Table I) where *B* is MF]. When $\mathbf{h}_1 = 0$ the local volume fraction $v(z) = v_c$ for all z [condition (iii c)], therefore, $\bar{\rho}_c = 0$ for all $z \gtrsim 0$ [as $\varepsilon(z,t) = \varepsilon_2$] and $\bar{\rho} \simeq \bar{\rho}_{\mathrm{BG}}$ for all t (horizontal dotted line in Fig. 2). The difference between the peak value $\bar{\rho}_{\mathrm{peak}}$ and $\bar{\rho}_{\mathrm{BG}}$ therefore provides a measure of the magnitude of $\mathbf{h}_1$ (Fig. 3); hence, the $\bar{\rho}$ data indicates that

$$\mathbf{h}_1(\mathrm{C11}) < \mathbf{h}_1(\mathrm{C12}) < 0 < \mathbf{h}_1(\mathrm{C13}) < \mathbf{h}_1(\mathrm{C14}), \qquad (30)$$

where $\mathbf{h}_1 = 0$ corresponds to an effective critical liquid mixture of C12.6 with critical temperature T_c(C12.6) = 35.4 °C (Fig. 3). A more precise quantification of $\mathbf{h}_1$ will be given in Sec. V.

The sign of $\mathbf{h}_1$ determines whether *n*-alkane ($\mathbf{h}_1 < 0$) or methyl formate ($\mathbf{h}_1 > 0$) preferentially adsorbs at the interface; while the magnitude of $\mathbf{h}_1$ determines the strength of this adsorption. For sufficiently large $\mathbf{h}_1$ the adsorption is described by the strong critical adsorption surface scaling function $P_\pm$ at all reduced temperatures t [11,12]; at somewhat smaller $\mathbf{h}_1$ values the scaling variable $y' = \mathbf{h}_1 t^{-\Delta_1}$ plays an important role. At sufficiently large y', corresponding to small t, $G'_\pm(x, y' \gg 1) \approx P_\pm(x)$ and the experimental data should be described by the ellipticity $\bar{\rho}_P$ calculated from the $P_\pm$ function. However, at small y', corresponding to large t, the experimental data should deviate significantly from $\bar{\rho}_P$; in this region the $G_\pm$ function (which differs from the $P_\pm$ function at small $z \lesssim l_h$, Fig. 1) plays an important role in

determining the shape of $\overline{\rho}$. In Fig. 2, we have plotted $\overline{\rho}_{P+}$ calculated from P_+ for the mixtures C11 and C12 (long dashed lines) where the $\overline{\rho}_{P+}$ curves have been shifted vertically so that a comparison can be made with the experimental data at small t. The C11 and C12 data are accurately described by $\overline{\rho}_{P+}$ for $t \lesssim 3\times10^{-3}$ and $t \lesssim 8\times10^{-4}$, respectively, in agreement with the above discussion. The ellipticity $\overline{\rho}_{P+}$ provides a better description of C11 up to larger t than C12 because $|\mathbf{h}_1\ (\mathrm{C11})| > |\mathbf{h}_1\ (\mathrm{C12})|$ [Eq. (30)].

Thus far, we have observed that the experimental data in the one-phase region qualitatively agrees with the expectations of the surface scaling function $G'_+(z/\xi_+, \mathbf{h}_1 t^{-\Delta_1})$. In order to proceed further, a specific theoretical model for $G_\pm$ (Sec. II) must be considered, where $\overline{\rho}$ is determined by numerically solving Maxwell's equations. Before this is possible we must first define the extrapolation length z_e, which appears in Eq. (19), and describe how the optical dielectric function on the vapor side of the interface at $z<0$ connects onto the weak critical adsorption function at $z>0$. As mentioned in Sec. II, the extrapolation length z_e ensures that the local order parameter at the surface $m_1 = m(z=0) \sim \mathbf{h}_1$ at small $\mathbf{h}_1$ [as required by condition (iii c)]; while at large $\mathbf{h}_1 (\to\infty)$, z_e limits $m(z=0) = M_- t^\beta P_\pm [z_e/\xi_\pm] \simeq M_- c_\pm (z_e/\xi_{o\pm})^{-\beta/\nu}$ to its maximum saturation value, namely, $m(z=0) = m_{\max} = 1 - v_c$. Hence, to a good approximation [33]

$$z_e \simeq \xi_{o\pm} \left(\frac{1-v_c}{M_- c_\pm} \right)^{-\nu/\beta} \quad (\sim 0.4 \text{ nm}), \tag{31}$$

where $c_\pm$ is defined in Eq. (10). The critical portion of the surface scaling function, which occupies $z \geqslant 0$, must join onto the dielectric profile, which describes the vapor side of the interface (at $z<0$) in a continuous fashion. This continuity in $\varepsilon(z)$ at $z=0$ is accomplished by assuming that the vapor side of the interface is given by

$$\varepsilon(z) = 1 + \frac{[\varepsilon(0)-1][1+e^{-z_e/\xi_{\mathrm{BG}}}]}{1+e^{-(z+z_e)/\xi_{\mathrm{BG}}}}, \quad z<0. \tag{32}$$

The noncritical correlation length ξ_{BG} is an adjustable parameter so that, for a particular G_+ model, $\overline{\rho}_{G+} = \overline{\rho}_{\mathrm{BG}}$ at large reduced temperature ($t \sim 0.1$), where the critical contribution ($\overline{\rho}_c$) is negligible.

We are now in a position to compare a model for the weak surface scaling function $G_\pm$ with experiment, where Eq. (32) describes $\varepsilon(z)$ for $z<0$ while Eqs. (25) and (6), with a model for $G_\pm$ [Eq. (15)], describes $\varepsilon(z)$ for $z>0$. A numerical solution of Maxwell's equations with this model $\varepsilon(z)$ determines the ellipticity $\overline{\rho}_G$ for each t, which can be compared with experimental data. Four length scales appear in this problem: (i) ξ_{o+}, which, as discussed above is determined by the position of the $\overline{\rho}$ peak in the one-phase region [Eq. (22)], but must also be consistent with the turbidity measurements (Table I); (ii) z_e, which is fixed by Eq. (31), where $c_\pm$ is taken from the $P_\pm$ model; (iii) l_{h+}, which determines the crossover from $G_+ \sim z^\kappa$ behavior (at small $z \lesssim l_{h+}$) to the P_+ surface scaling function (at large $z \gtrsim l_{h+}$); and (iv) ξ_{BG}, which is slightly correlated with l_{h+}, but to a good approximation is determined by $\overline{\rho}_{\mathrm{BG}}$ to within 10%.

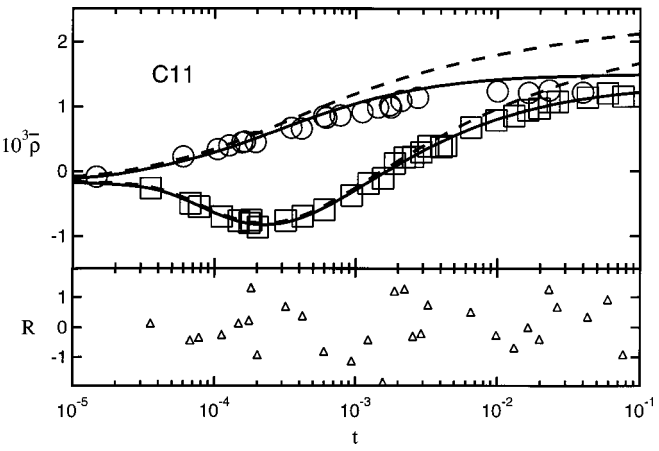

FIG. 4. Comparison of the ellipticity $\overline{\rho}$ for the C11 mixture with various theoretical models. Experiment: one-(squares) and two-phase (circles) data. Theory: $P_\pm$ (dashed lines) and $G_\pm$ (solid lines) models. The residuals $R = (\overline{\rho}_i - \overline{\rho}_{Gi})/s_{\min}$ are also shown for the $G_\pm$ model (triangles) in the one-phase region.

Hence, ξ_{o+} and ξ_{BG} are constrained within rather tight bounds; thus, only l_{h+} is a completely adjustable parameter with which to improve the agreement between theory and experiment. It is important to note that once ξ_{o+}, ξ_{BG}, and l_{h+} are determined from the one-phase data, there are *no* adjustable parameters in the two-phase region because ξ_{o-} and l_{h-} are determined by the universal amplitude ratio $\xi_{o+}/\xi_{o-} = l_{h+}/l_{h-} = R_\xi$ ($\simeq 1.96$ [5]). Additionally, it is not possible to have differing values for ξ_{BG} in the one- and two-phase region because this would lead to a discontinuity in $\overline{\rho}_G$ at T_c, in disagreement with condition (iv) [54]. Hence, in the following we have adjusted l_{h+}, ξ_{o+}, and ξ_{BG} to provide the best agreement in the one-phase region where ξ_{o+} and ξ_{BG} are constrained by the turbidity and $\overline{\rho}_{\mathrm{BG}}$ results, respectively; these values for l_{h+}, ξ_{o+}, and ξ_{BG} are then used in the two-phase region to evaluate the two-phase model.

The optimal values for $(\xi_{o+}, \xi_{\mathrm{BG}}, l_{h+})$ are listed in Table II. These values were determined by searching the three-dimensional space $(\xi_{o+}, \xi_{\mathrm{BG}}, l_{h+})$ for the lowest standard deviation $s_{\min}$ [55] where $s^2 = \Sigma_i (\overline{\rho}_i - \overline{\rho}_{Gi})^2/(N-3)$, $\overline{\rho}_i$ and $\overline{\rho}_{Gi}$ represent the experimental and calculated ellipticity for data point i, N is the total number of data points for a particular liquid mixture, and the number of adjustable parameters is three. In Fig. 4, the mixture C11 is compared with $\overline{\rho}_P$ (dashed lines) and $\overline{\rho}_G$ (solid lines) in both the one- (open squares) and two-phase (open circles) regions. As expected, the $P_\pm$ model only provides a good description of the experimental data close to T_c; the deviations observed far from T_c are well described by the $G_\pm$ surface scaling function [Eq. (15)] as indicated by the residuals $R = (\overline{\rho}_i - \overline{\rho}_{Gi})/s_{\min}$ (in the one-phase region), which are randomly distributed about zero for all reduced temperatures t. The $G_\pm$ model is compared with the mixtures C12, C13, and C14 in Fig. 5 where the meaning of the symbols and lines are identical to Fig. 4, except that the stable (metastable) critical adsorption data is

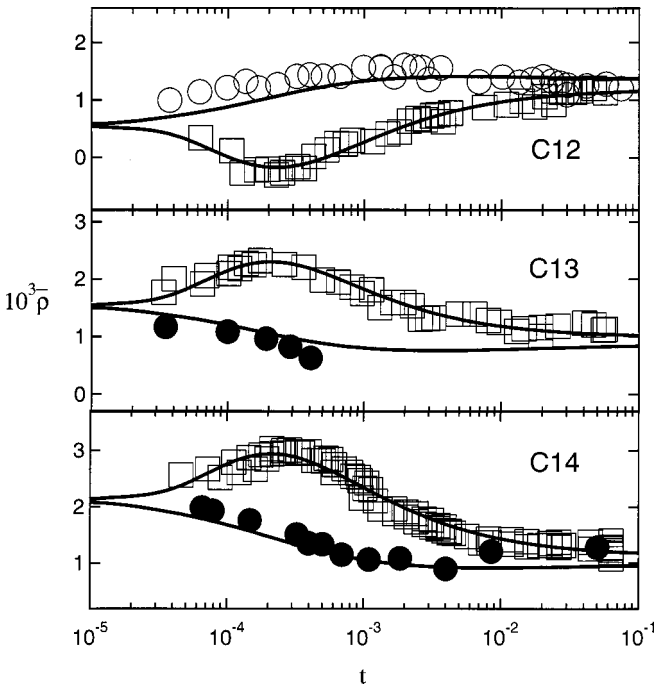

FIG. 5. Comparison of the ellipticity $\bar{\rho}$ for the C12, C13, and C14 mixtures. Experiment: one- (squares) and two-phase (circles) data where the open (solid) symbols represent stable (metastable) data. Theory: $G_{\pm}$ model (solid lines).

represented by an open (solid) symbol in this figure. The one-phase residuals for C12, C13, and C14 (which are not shown) are also randomly distributed about zero, indicating a good fit for all reduced temperatures *t*, in agreement with the results of C11.

It is really rather surprising that the metastable two-phase data for C13 and C14 (Fig. 5, solid circles) is well described by the G_- model. This is because, in our opinion (as expressed earlier in [33]), the P_- function used for these mixtures should be somewhat different from the form that we have assumed (i.e., the P3a model from [12]). This can be understood as follows. Throughout this paper $v(z)$ represents the adsorbed component at the liquid-vapor surface. For C11 and C12 the *n*-alkane adsorbs at the liquid-vapor surface, but also, the *n*-alkane is lighter than methyl formate; hence $v(z)$ will obey the equation

$$v(z)=v_c+M_-t^{\beta}P_-(z/\xi_-), \tag{33}$$

where $P_-(z)\to 1$ as $z\to\infty$. This situation, where the lighter component adsorbs at the liquid-vapor surface, is identical to the conditions studied in [11,12] (from which the P3a model was derived). However, for C13 and C14, methyl formate adsorbs at the liquid-vapor surface; $v(z)$ now represents the local volume fraction of methyl formate, which is the *minority* component in the upper phase, hence $v(\infty)=v_c-M_-t^{\beta}$ *in the bulk*. If Eq. (33) is retained with $P_-(x)\sim x^{\beta/\nu}$ for $x \lesssim 1$ [Eq. (10)], then $P_-(z)\to -1$ (rather than $+1$) as $z\to\infty$ [56]. Hence, in our opinion, there should be two forms for P_-, specifically, P_-^L (P_-^H) corresponding to adsorption of the light (heavy) component at the liquid-vapor surface. P_-^L was characterized in [11,12]. P_-^H has not yet been characterized, but could be studied in systems where the surface tensions $\sigma_H<\sigma_L$ and the optical refractive indices $n_H>n_L$ so that adsorption (rather than wetting [41]) of component *H* is found at the liquid-vapor surface in the two-phase regime. This situation is somewhat analogous to that studied in [57,58] where the surface energy σ_- between a critical mixture and a noncritical wall differed in the light and heavy phases within the two-phase region. Similarly $v(z)$, and hence P_-, should differ in the light and heavy phases because $\sigma_-\sim\int(dv(z)/dz)^2\,dz$ [59] at least in mean field theory.

V. THE SURFACE FIELD $\mathbf{h_1}$

According to Eqs. (7) and (21), which we restate here for convenience,

$$l_{h+}=\xi_{o+}|\mathbf{h}_1|^{-\nu/\Delta_1}, \quad \text{where } \mathbf{h}_1=(\sigma_A-\sigma_B)l_\sigma^2/k_BT_c.$$

Here σ_A (σ_B) is the surface energy of the *n*-alkane (methyl formate) *within* the liquid mixture, l_σ is a molecular length scale (whose value should depend upon the particular liquid mixture or homologous series being studied), and the sign of $\mathbf{h}_1$ determines whether the *n*-alkane ($\mathbf{h}_1<0$) or methyl formate ($\mathbf{h}_1>0$) component preferentially adsorbs at the liquid-vapor surface. Therefore, l_{h+} exhibited in Table II for the different liquid mixtures should be related to the surface energy difference $\Delta\sigma=\sigma_A-\sigma_B$. Alternatively,

$$\Omega=(l_{h+}/\xi_{o+})^{-\Delta_1/\nu} \tag{34}$$

should be proportional to

$$\Sigma=|\sigma_A-\sigma_B|/k_BT_c \tag{35}$$

with a proportionality constant of l_σ^2, where l_σ is expected to be approximately constant for a given homologous series of critical liquid mixtures. A difficulty that arises in testing the correspondence between Eqs. (34) and (35) is that σ_A and σ_B represent the surface energies *within the liquid mixture*. However, if σ_A^* and σ_B^* represent the surface tensions of the *pure components at* T_c, then

$$\Delta\sigma=\sigma_A^*-(\sigma_B^*+\sigma_o^*) \tag{36}$$

is expected to be a reasonable approximation where σ_o^* is a surface tension offset applied to methyl formate which ensures that $\Delta\sigma=0$ at $\mathbf{h}_1=0$, as described below. From Fig. 3, $\mathbf{h}_1=0$ (where $\bar{\rho}=\bar{\rho}_{\rm BG}$ for all *t*) occurs at an effective liquid mixture of C12.6 (vertical dashed line) with T_c(C12.6) $=35.4\,^\circ$C. In Fig. 6, σ^* for the pure components [60] is plotted as a function of temperature where the crosses on each of the curves indicate the critical temperature for each of the four liquid mixtures. In order that $\mathbf{h}_1=0$ for C12.6 with T_c (C12.6) $=35.4\,^\circ$C the surface tension for pure methyl formate, σ_B^*, would have to be shifted up by a value of $\sigma_o^*=1.64\,\mathrm{erg/cm^2}$ (dashed line in Fig. 6). Thus, $\Delta\sigma(T_c)$, at the critical temperature for each of the liquid mixtures, can be found by determining the difference in surface energies

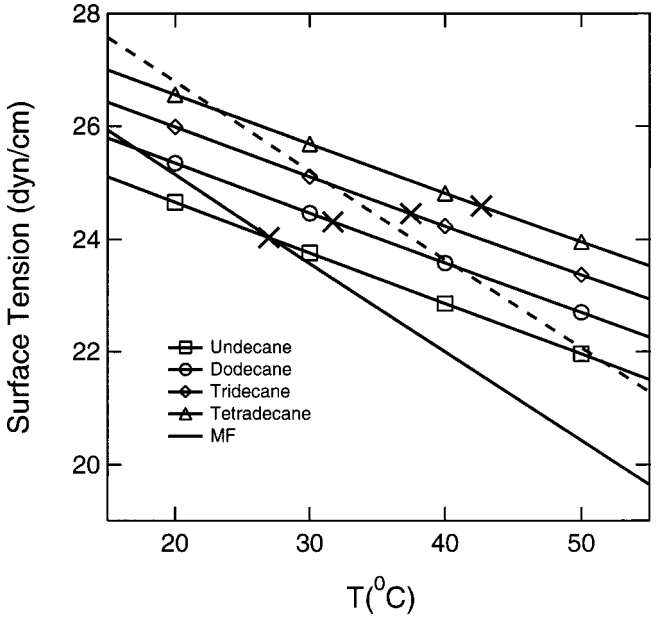

FIG. 6. Surface tension σ^* of the pure liquid components from [60]. The crosses on each of the C11 to C14 curves are positioned at the measured T_c for the *n*-alkane and MF mixture. The dashed line corresponds to the MF data when offset by $\sigma_0^* = 1.64\ \mathrm{erg/cm^2}$. The difference between the dashed line and crosses provides a measure of the surface tension difference $\Delta\sigma = \sigma_A - \sigma_B$ (Table I) where $\Delta\sigma = 0$ for an effective mixture of C12.6 at T_c (C12.6) = 35.4 °C.

between the dashed line and each of the crosses in Fig. 6; these values for $\Delta\sigma(T_c)$ are listed in Table I. In Fig. 7, $|\sigma_A - \sigma_B|/k_B T_c$ is plotted against $(l_{h+}/\xi_{o+})^{-\Delta_1/\nu}$ for each liquid mixture. A linear fit to this data set (solid line), which has been constrained to pass through the origin so that $\Delta\sigma = 0$ when $\mathbf{h}_1 = 0$ (corresponding to $l_{h+} = \infty$), has a slope of $l_\sigma^2 = (4.6 \pm 0.4\ \text{Å})^2$ for the $G_\pm$ model. Hence, as expected, l_σ is of the order of a molecular length.

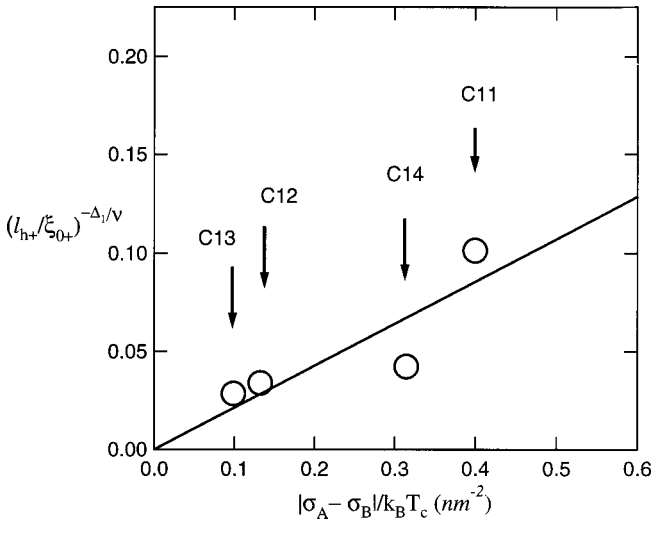

FIG. 7. Plot of $(l_{ht}/\xi_{0+})^{-\Delta_1/\nu}$ versus $|\sigma_A - \sigma_B|/k_B T_c$ for the $G_\pm$ model (circles). The solid line represents a linear fit through this data set with the constraint that the line passes through the origin to ensure that $\mathbf{h}_1 = 0$ ($l_{h+} \to \infty$) when $\sigma_A = \sigma_B$. The slope of the line gives l_σ^2 (Table II).

VI. CONCLUSION

In this paper we have used a homologous series of critical *AB* binary liquid mixtures, *n*-alkane (*A*) and methyl formate (*B*), to investigate the weak critical adsorption regime at the liquid-vapor surface. In this regime the surface energy $\sigma_A \approx \sigma_B$, thus, the surface field $\mathbf{h}_1 \sim \Delta\sigma$ ($= \sigma_A - \sigma_B$) is small and the adsorption of both components is almost equally probable. As the *n*-alkane component is varied from *n*-undecane (C11) to *n*-tetradecane (C14) the surface preference changes from *n*-alkane for C11 and C12 ($\mathbf{h}_1 < 0$) to methyl formate for C13 and C14 ($\mathbf{h}_1 > 0$). A point of equally probable adsorption for the two components corresponding to $\mathbf{h}_1 = 0$ would occur for an ''effective'' critical mixture of C12.6 and methyl formate. The surface composition with depth into the critical liquid mixture is governed by a universal surface scaling function $G_\pm(x,y)$, which depends upon two dimensionless length scales $x \sim z/\xi_\pm$ and $y \sim z/l_{h\pm}$ [Eq. (19)], where $l_{h\pm}$ [$\sim |\mathbf{h}_1|^{-\nu/\Delta_1}$, Eq. (7)] is a new length scale associated with the $\mathbf{h}_1$ field. For sufficiently small $\mathbf{h}_1$, $l_{h_\pm}$ can become quite large and, under certain circumstances, comparable to the bulk correlation length $\xi_\pm$. Hence the weak critical adsorption behavior is a sensitive function of $\mathbf{h}_1$ in this regime, and as a consequence, the C11 to C14 mixtures exhibit rather different adsorption behaviors. A theoretical model [Eqs. (15)–(21)], which conforms with the theoretical predictions (i)–(v) contained within Sec. II, provides an excellent description of the experimental data in both the one- and two-phase regions (Figs. 4 and 5, solid lines) where the optimal fitting parameters are listed in Table II. The surface field length l_{h+} is expected to be related to the surface energy difference $\Delta\sigma$ ($\sim \mathbf{h}_1$); this interrelationship is examined in Sec. V and Fig. 7 from which the molecular surface length $l_\sigma \sim 5$ Å (Table II), characteristic of this particular homologous series, is extracted.

The results in this paper now allow us to provide some guidance as to when weak surface field effects will be important for critical adsorption. In accordance with a suggestion in [19], the strong critical adsorption surface scaling function $P_\pm$ describes the critical adsorption data in Fig. 2 for $t < t_x$ while the weak critical adsorption surface scaling function $G_\pm$ is required for $t \gtrsim t_x$ where the ''crossover'' temperature t_x is defined by

$$|\mathbf{h}_1| t_x^{-\Delta_1} \simeq 1. \tag{37}$$

Combining Eq. (37) with Eq. (21) leads to

$$|\Delta\sigma| = \frac{t_x^{\Delta_1} k_B T_c}{l_\sigma^2}. \tag{38}$$

Hence, the strong critical adsorption surface scaling function $P_\pm$ can be used at all accessible temperatures ($t_x \simeq 0.1$) for room temperature critical binary liquid mixtures ($T_c = 300$ K) provided that $|\Delta\sigma| \gtrsim 6\ \mathrm{erg/cm^2}$. Similarly, Eq. (38) also provides a criterion for when the $\overline{\rho}$ peak position can be described by Eq. (22). Equation (22) will start to fail when the peak reduced temperature $t_{\mathrm{peak}} = t_x$, hence, from Eqs. (22) and (38) this occurs when

$$|\Delta\sigma| = \frac{k_B T_c}{l_\sigma^2}\left(\frac{\xi_{o+}}{0.064\lambda}\right)^{\Delta_1/\nu}. \quad (39)$$

According to this equation (and using data from this paper), Eq. (22) can be used to accurately determine the correlation length amplitude ξ_{o+} from ellipsometric critical adsorption data for room temperature critical binary liquid mixtures provided that $|\Delta\sigma| \gtrsim 0.2\ \mathrm{erg/cm^2}$.

ACKNOWLEDGMENT

This research was supported by the National Science Foundation through Grant No. DMR-0097119.

[1] H. W. Diehl, in *Phase Transitions and Critical Phenomena*, edited by C. Domb and J. L. Lebowitz (Academic, London, 1986), Vol. 10.
[2] K. Binder, in *Phase Transitions and Critical Phenomena*, edited by C. Domb and J. L. Lebowitz (Academic, London, 1983), Vol. 8.
[3] S. Dietrich, in *Phase Transitions and Critical Phenomena*, edited by C. Domb and J. L. Lebowitz (Academic, London, 1987), Vol. 12.
[4] M. E. Fisher and J.-H. Chen, J. Phys. (France) **46**, 1645 (1985).
[5] Here we ignore the small differences in value between the true correlation length [H. B. Tarko and M. E. Fisher, Phys. Rev. Lett. **31**, 926 (1973)] and the second moment of the bulk correlation length [A. J. Liu and M. E. Fisher, Physica A **156**, 35 (1989); C. Ruge, P. Zhu, and F. Wagner, *ibid.* **209**, 431 (1994)]. A recent interpolation scheme [G. Flötter and S. Dietrich, Z. Phys. B: Condens. Matter **97**, 213 (1995)] indicated a considerably lower value for this ratio of $R_\xi = 1.73 \pm 0.04$ for the true correlation length.
[6] M. E. Fisher and P.-G. de Gennes, C. R. Seances Acad. Sci., Ser. B **287**, 207 (1978).
[7] A. J. Liu and M. E. Fisher, Phys. Rev. A **40**, 7202 (1989).
[8] H. W. Diehl and M. Smock, Phys. Rev. B **47**, 5841 (1993); **48**, 6740(E) (1993).
[9] M. Smock, H. W. Diehl, and D. P. Landau, Ber. Bunsenges. Phys. Chem. **98**, 486 (1994).
[10] Z. Borjan and P. J. Upton, Phys. Rev. E **63**, 065102 (2001).
[11] J. H. Carpenter, B. M. Law, and D. S. P. Smith, Phys. Rev. E **59**, 5655 (1999).
[12] J. H. Carpenter, J.-H. J. Cho, and B. M. Law, Phys. Rev. E **61**, 532 (2000).
[13] S. B. Kiselev, J. F. Ely, and M. Yu. Belyakov, J. Chem. Phys. **112**, 3370 (2000).
[14] U. Ritschel and P. Czerner, Phys. Rev. Lett. **77**, 3645 (1996).
[15] N. S. Desai, S. Peach, and C. Franck, Phys. Rev. E **52**, 4129 (1995).
[16] A. Ciach and U. Ritschel, Nucl. Phys. B **489**, 653 (1997).
[17] P. Czerner and U. Ritschel, Physica A **237**, 240 (1997).
[18] P. Czerner and U. Ritschel, Int. J. Mod. Phys. B **11**, 2075 (1997).
[19] A. Ciach, A. Maciolek, and J. Stecki, J. Chem. Phys. **108**, 5913 (1998).
[20] J.-H. J. Cho and B. M. Law, Phys. Rev. Lett. **86**, 2070 (2001).
[21] H. W. Diehl, Int. J. Mod. Phys. B **11**, 3503 (1997).
[22] B. M. Law, Prog. Surf. Sci. **66**, 159 (2001).
[23] D. P. Landau and K. Binder, Phys. Rev. B **41**, 4633 (1990); C. Ruge, S. Dunkelmann, and F. Wagner, Phys. Rev. Lett. **69**, 2465 (1992).
[24] T. W. Burkhardt and H. W. Diehl, Phys. Rev. B **50**, 3894 (1994).
[25] P. J. Upton, Phys. Rev. Lett. **81**, 2300 (1998).
[26] H. W. Diehl and M. Shpot, Nucl. Phys. B **528**, 595 (1998).
[27] M. E. Fisher suggested the name "normal."
[28] A. J. Bray and M. A. Moore, J. Phys. A **10**, 1927 (1977).
[29] C. Franck and S. E. Schnatterly, Phys. Rev. Lett. **48**, 763 (1982); J. A. Dixon, M. Schlossman, X.-L. Wu, and C. Franck, Phys. Rev. B **31**, 1509 (1985); M. Schlossman, X.-L. Wu, and C. Franck, *ibid.* **31**, 1478 (1985).
[30] D. S. P. Smith, B. M. Law, M. Smock, and D. P. Landau, Phys. Rev. E **55**, 620 (1997).
[31] H. Zhao, A. Penninckx-Sans, L.-T. Lee, D. Beysens, and G. Jannink, Phys. Rev. Lett. **75**, 1977 (1995); J. R. Howse, J. Bowers, E. Manzanares-Papayanopoulos, I. A. McLure, and R. Steitz, Phys. Rev. E **59**, 5577 (1999); J. Jestin, L.-T. Lee, M. Privat, and G. Zalczer, Eur. Phys. J. B (to be published).
[32] D. Beysens and S. Leibler, J. Phys. (France) Lett. **43**, L133 (1982).
[33] D. S. P. Smith and B. M. Law, Phys. Rev. E **52**, 580 (1995).
[34] D. S. P. Smith and B. M. Law, Phys. Rev. E **54**, 2727 (1996).
[35] L. Sigl and W. Fenzl, Phys. Rev. Lett. **57**, 2191 (1986).
[36] D. J. Durian and C. Franck, Phys. Rev. Lett. **59**, 555 (1987).
[37] Surface tension measurements are primarily sensitive to the *first surface layer* [P. Mach, C. C. Huang, and H. T. Nguyen, Phys. Rev. Lett. **80**, 732 (1998)]. Hence, for critical binary liquid mixtures, surface tension measurements are expected to probe ordinary surface critical exponents.
[38] $\Delta_1^{\mathrm{ex}} = \nu(d - \eta_\parallel)/2$ [26] and $\eta_\parallel = d + 2$ [25,28] hence $\Delta_1^{\mathrm{ex}} = -\nu = -0.632$.
[39] A. Maciolek, A. Ciach, and A. Drzewiński, Phys. Rev. E **60**, 2887 (1999).
[40] At T_c, the continuity of $P_\pm$ yields $c_+/c_- = (\xi_{o+}/\xi_{o-})^{-\beta/\nu}$ [8] according to Eq. (10).
[41] For an *AB* critical liquid mixture where the density $\rho_A < \rho_B$, critical adsorption of component *A* will be found in both the one- and two-phase regimes if the surface tension $\sigma_A < \sigma_B$ (this is the situation studied in [11,12,30,33,34]). If $\sigma_A > \sigma_B$, then the situation is more complicated. Critical adsorption of component *B* is found in the one-phase region. In the two-phase region, either critical adsorption or wetting of component *B* can be found. Wetting will be found provided that the long-range dispersion interaction is *positive* (at the liquid-vapor interface this is achieved for an optical refractive index $n_B < n_A$, giving rise to a positive Hamaker constant) and that one is *above* the wetting transition temperature. If either of

these two conditions is not fulfilled, then critical adsorption of component *B* will occur [22].
[42] D. Beysens, A. Bourgou, and P. Calmettes, Phys. Rev. A **26**, 3589 (1982).
[43] L. W. DaMore and D. T. Jacobs, J. Chem. Phys. **97**, 464 (1992).
[44] D. Beaglehole, in *Fluid Interfacial Phenomena*, edited by C. A. Croxton (Wiley, New York, 1985).
[45] D. Beaglehole, Physica B & C **100**, 163 (1980).
[46] D. Ross, D. Bonn, and J. Meunier, Nature (London) **400**, 737 (1999).
[47] J.-H. J. Cho and B. M. Law (unpublished).
[48] B. M. Law, Phys. Rev. Lett. **69**, 1781 (1992); **70**, 3359(E) (1993); B. M. Law and H. K. Pak, J. Chem. Phys. **106**, 301 (1997).
[49] R. F. Kayser, Phys. Rev. B **34**, 3254 (1986).
[50] B. M. Law and D. Beaglehole, J. Phys. D **14**, 115 (1981).
[51] M. Born and E. Wolf, *Principle of Optics* (Pergamon, Oxford, 1980), Sec. 1.6.
[52] P. K. L. Drude, *The Theory of Optics* (Dover, New York, 1959), p. 292.
[53] J. Lekner, *Theory of Reflection* (Martinus Nijhoff, Dordrecht, 1987).
[54] Differing values of ξ_{BC}, in the one- and two-phase regions, would lead to differing $\overline{\rho}_{\mathrm{BG}}$ values in the two regions. $\overline{\rho}_{\mathrm{BG}}$ is, to a good approximation, an additive constant that is essentially independent of t [33,34]. It merely shifts the whole $\overline{\rho}$ curve vertically, without any change in shape. Therefore, differing vertical shifts in the one- and two-phase regions would generate a discontinuity in $\overline{\rho}_G$ at T_c.
[55] P. R. Bevington, *Data Reduction and Error Analysis for the Physical Sciences* (McGraw-Hill, New York, 1969).
[56] This problem cannot be resolved by changing the + sign to a − sign in Eq. (33). In this case, although $P_-(z)\rightarrow+1$ as $z\rightarrow\infty$, we would now have to change $P_-(x)\sim x^{-\beta/\nu}$ to $P_-(x)\sim -x^{-\beta/\nu}$ for small x in order that $v(z)$ approach its saturated value at the surface $[v(0)\approx 1]$.
[57] M. E. Fisher and P. J. Upton, Phys. Rev. Lett. **65**, 2402 (1990); **65**, 3405 (1990).
[58] T. Mainzer-Althof and D. Woermann, Physica A **234**, 623 (1997).
[59] J. S. Rowlinson and B. Widom, *Molecular Theory of Capillarity* (Oxford University Press, London, 1982), Chap. 3.
[60] J. J. Jasper, J. Phys. Chem. Ref. Data **1**, 841 (1972).
[61] J. Timmermans, *Physico-Chemical Constants of Pure Organic Compounds* (Elsevier, New York, 1950).